International Journal of Computer Information Systems and Industrial Management Applications
ISSN 2150-7988 Volume 18 (2026) pp. 1-18

https://doi.org/10.70917/ijcisim-2026-0156
Article

Research on the Prediction of Emergency Response Time for Public Emergencies Based on Long and Short-Term Memory Network Models

Runhang Zhang *

Shaanxi Police College, Xi'an, Shaanxi, 710000, China; mkb68857@163.com

Abstract: Efficient emergency response to public emergencies is key to minimizing social losses. This study proposes an ARIMA-LSTM combined measurement model. By employing an optimal weighted combination prediction method, the model integrates the linear trend analysis capabilities of the ARIMA model with the nonlinear time-series dependency learning advantages of the long short-term memory (LSTM) network. This approach extracts the linear and nonlinear features from public emergency response time prediction data, addressing the issue of low simulation accuracy in standalone ARIMA and LSTM models. The experimental results show that the prediction performance of the BP neural network, single ARIMA model, and LSTM model are all inferior to the ARIMA-LSTM combination model. When applying the model in this paper to predict the emergency response time for public emergencies in multiple regions, the average emergency response time is only 2.3 hours, and the positive rate of suspected events and outbreak events in early warning signals is less than 5%, indicating that the model in this paper has a low false alarm rate and high practicality. This provides a reliable path for improving the efficiency of emergency response departments and reducing social losses.

Keywords: ARIMA; LSTM; ARIMA-LSTM combined measurement model; public emergency response time prediction

1. Introduction

A public emergency refers to an unexpected event that causes or may cause significant loss of life, property damage, ecological destruction, and severe social harm, thereby threatening public safety [1-3]. Based on the nature and scope of the event, public emergencies can be categorized into four types: natural disasters, accidents, public health incidents, and social security incidents [4-6]. In our daily lives, public emergencies occur frequently. To effectively respond to various public emergencies, minimize losses, ensure public safety, and maintain social stability, long short-term memory (LSTM) network models are widely applied in the prediction of public emergencies [7-10].

The Long Short-Term Memory (LSTM) model is a special type of Recurrent Neural Network (RNN). Compared to traditional RNN models, the LSTM model introduces a gating mechanism to better capture long-term dependencies in time series data, thereby achieving better performance when processing sequence data [11-14]. Additionally, the LSTM model possesses strong memory capabilities, enabling it to flexibly remember and forget historical information [15]. Therefore, applying LSTM models to the prediction of emergency response times for public emergencies is expected to yield more accurate and reliable prediction results [16-17]. However, relying solely on LSTM model predictions is insufficient to ensure effective response and handling of emergencies. It is also necessary to evaluate and summarize the performance of these models to continuously improve and enhance emergency response capabilities [18-20].

Literature [21] highlights the severity of influenza as a public emergency and emphasizes that early prediction is an effective method for controlling influenza outbreaks. Based on influenza outpatient data

collected from the Taiwan Centers for Disease Control, LSTM was used to determine the correlation between short-term prediction and outbreak calculation methods. Literature [22] highlights air pollution as a global concern and proposes an LSTM method for predicting air quality. Through research on air quality data from Beijing, China, it demonstrates that this method outperforms traditional methods in predicting PM2.5, PM10, and CO concentrations. Literature [23] introduces LSTM and the severe negative impacts of COVID-19. The results of using LSTM overlay show that the R^2 values for confirmed COVID-19 cases and confirmed deaths are 0.9625 and 0.9656, respectively, outperforming combinations of other evaluation models. Literature [24] proposes an emergency event prediction scheme that models the correlation between spatial and temporal domains using spatial segmentation and LSTM neural networks, with a focus on emergency situations in Brazil. Through comparison, it is demonstrated that the LSTM network outperforms other methods in prediction. Literature [25] points out that when sudden events are widely discussed, it can lead to negative emotions. Therefore, an IPSO-LSTM hybrid prediction model was constructed to predict and analyze the trend of public opinion propagation during sudden events. Experimental results show that this model outperforms other models and has high prediction accuracy. Literature [26] introduces a pioneering method combining time series ratio analysis with the Long Short-Term Memory (TG-LSTM) model, aiming to provide early financial warnings for businesses. It demonstrates the effectiveness of the TG-LSTM model, achieving significant progress in advancing financial risk prediction. Literature [27] introduces a new public affairs distribution method based on Chicago crime data, utilizing LSTM, multi-layer perceptron (MLP), and their integration, demonstrating that the hybrid LSTM-MLP model achieves higher predictive accuracy than standalone LSTM or MLP models.

To address the challenge of high social losses caused by delays in emergency response to public emergencies, this paper proposes an ARIMA-LSTM model framework. The ARIMA model is used to extract the linear components from the time series data of emergency response times for public emergencies. Then, the LSTM model is used to fit the residuals of the ARIMA model, extracting the nonlinear components from the time series data of emergency response times for public emergencies to obtain more accurate prediction results. The performance of the model is validated through comparative experiments with various single models, and the emergency response data for public emergencies in City P from 2010 to 2024 is selected to verify the specific prediction effectiveness of the model.

2. Public Emergency Prediction Based on ARIMA-LSTM

2. Public Emergency Prediction Based on ARIMA-LSTM

2.1.1. ARIMA Forecasting Model and Theory

The ARIMA model [28] consists of three parts, namely autoregression (AR), integration (I), and moving average (MA), which are defined as follows: AR represents autoregression. I represents the order of integration. MA represents the moving average model.

(1) AR model

The AR model refers to a situation where the current value of a time series is determined solely by the past values of the time series. The mathematical expression is as follows:

$$y_t = \alpha_0 + \alpha_1 y_{t-1} + \alpha_2 y_{t-2} + \cdots + \alpha_p y_{t-p} + \varepsilon_t \tag{1}$$

Where α_0 represents the constant term, $\alpha_1, \alpha_2 \cdots \alpha_p$ represent the coefficients of the autoregressive terms of each order, ε_t represents an independent white noise sequence, y_t represents the current forecast value, and $y_{t-1}, y_{t-2}, \cdots y_{t-p}$ represent the time series values at past time points. The AR model is determined solely by previous time series values and residuals. Among time series models, autoregressive models are relatively simple and are frequently used in practical applications, often serving as comparison models.

(2) MA model

MA model is completely unrelated to previous time series values. It is a linear model that predicts the current value using a linear combination of the current ε_t and the weighted average of the random errors $\{\varepsilon_t\}$ from the past q time points. The mathematical expression can be represented as:

$$y_t = \varepsilon_t + \theta_1 \varepsilon_{t-1} + \cdots + \theta_q \varepsilon_{t-q} \tag{2}$$

In this model, q is referred to as the order of the moving average model, denoted as the $MA(q)$ model, where $\theta_1, \theta_2 \ldots \theta_q$ are the moving average coefficients, and $\{\varepsilon_t\}$ is the sequence of random disturbance terms at different time periods. When $\theta_0 = 0$, it is referred to as the $MA(q)$ model.

(3) ARMA model

The ARMA model is a new model obtained by recombining the AR model and the MA model. This model is a linear model that combines previous time series values and residual sequences. The mathematical expression can be represented as:

$$y_t = \alpha_0 + \alpha_1 y_{t-1} + \alpha_2 y_{t-2} \ldots + \alpha_p y_{t-p} + \varepsilon_t - \beta_1 \varepsilon_{t-1} - \beta_2 \varepsilon_{t-2} \ldots - \beta_q \varepsilon_{t-q} \quad (3)$$

p is the autoregressive order, and q is the moving average order, abbreviated as the $ARMA(p,q)$ model. Among them, $\alpha_0, \alpha_1, \alpha_2, \ldots \alpha_p$ and $\beta_1, \beta_2, \ldots, \beta_q$ are parameters.

(4) ARIMA model

AR, MA, and ARMA models are all applicable to stationary random processes, but the public emergency monitoring data time series obtained in our actual work are non-stationary sequences. To address non-stationary sequences, the ARIMA model was developed. The ARIMA model can be viewed as a differentiated ARMA model, and its mathematical expression is:

$$\Phi(B)\nabla^d y_t = \Theta(B)\varepsilon_t \quad (4)$$

Among them, d is the difference order, $\Phi(B) = 1 - \phi_1 B - \cdots - \phi_p B^p$ represents the autoregressive coefficient polynomial, and $\Theta(B) = 1 - \theta_1 B - \cdots - \theta_q B^q$ represents the moving average coefficient polynomial.

2.1.2. Construction of the ARIMA model

The steps for constructing an ARIMA model can be divided into several steps: time series stationarity testing, non-stationary sequence processing, pattern recognition, model optimization, and model verification.

(1) Time series stationarity testing

Stationarity testing is to determine whether the current time series will continue with the existing trend for a period of time in the future. If the current time series has this trend in the future, then its research and analysis will be meaningful. A stationary time series is one in which the statistical properties such as mean, variance, and covariance are constant. The main methods for testing stationarity are graphical testing and the ADF unit root test.

The graphical test method involves observing the time series chart. If the time series fluctuates randomly around a certain mean, then the series is a stationary series. If the curve of the series does not show a fixed trend and the mean and variance vary greatly, then the public emergency monitoring series is a non-stationary series.

The ADF unit root test involves first assuming that the series contains a unit root. If the test statistic obtained from the ADF test is significantly smaller than the critical value corresponding to 1%, it indicates that the public emergency time series is stationary.

(2) Handling non-stationary series

After testing the stationarity of the time series, if the series is non-stationary, differencing operations must be performed.

(3) Pure randomness test

After testing for stationarity, the time series must also undergo a pure randomness test (also known as a white noise test) to determine whether there is any correlation between the time series and whether the historical values of the time series have any impact on future values. If the historical values of the time series have no influence on future trends, it indicates that the time series has no research value, and the construction of the model can be terminated.

(4) Model identification

Pattern recognition involves selecting a model from AR, MA, and ARMA models that better fits the time series trend. The specific process is determined using the properties of the autocorrelation coefficient and partial autocorrelation coefficient. If the partial autocorrelation function is truncated at p and the autocorrelation function tends to zero, then the autoregressive model $AR(p)$ should be selected. If the autocorrelation function is truncated at q and the partial correlation function tends

toward zero, then the moving average model $MA(q)$ should be selected. If neither the autocorrelation nor the partial correlation function is truncated and both function values tend toward zero, then the ARMA model $ARMA(p,q)$ should be selected.

However, this method may yield multiple combinations of values for p and q, so multiple tests are generally required to obtain the optimal combination and thus the optimal model.

(5) Model optimization

Model optimization is generally achieved by comparing the AIC and BIC values to select the optimal model. In general, AIC is defined as:

$$AIC = 2k - 2\ln(L) \tag{5}$$

where k is the number of model parameters and L is the likelihood function.

In general, BIC is defined as:

$$BIC = k\ln(n) - 2\ln(L) \tag{6}$$

Among them, K and L have the same meanings as in AIC, and n is the sample size.

The AIC criterion finds the optimal parameters of a model by balancing the complexity of the model and the likelihood function. The BIC expression adds the sample size to the AIC, which prevents the model complexity from increasing when the sample size is too large in order to improve accuracy. Therefore, the BIC criterion is more suitable for large sample sizes.

(6) Model testing

Model validation involves conducting significance tests and parameter tests on the model.

Significance testing of the model involves checking whether the model can fully explain the correlation in the time series. If the residual series of the time series is a white noise series, the test is passed; otherwise, the model must be refitted and validated again.

Parameter testing of the model involves removing those dependent variables that have little impact on the results, thereby simplifying the model as much as possible.

(7) Model Prediction

Input the time interval to be predicted for public emergency response time prediction analysis. The model prediction process is shown in Figure 1.

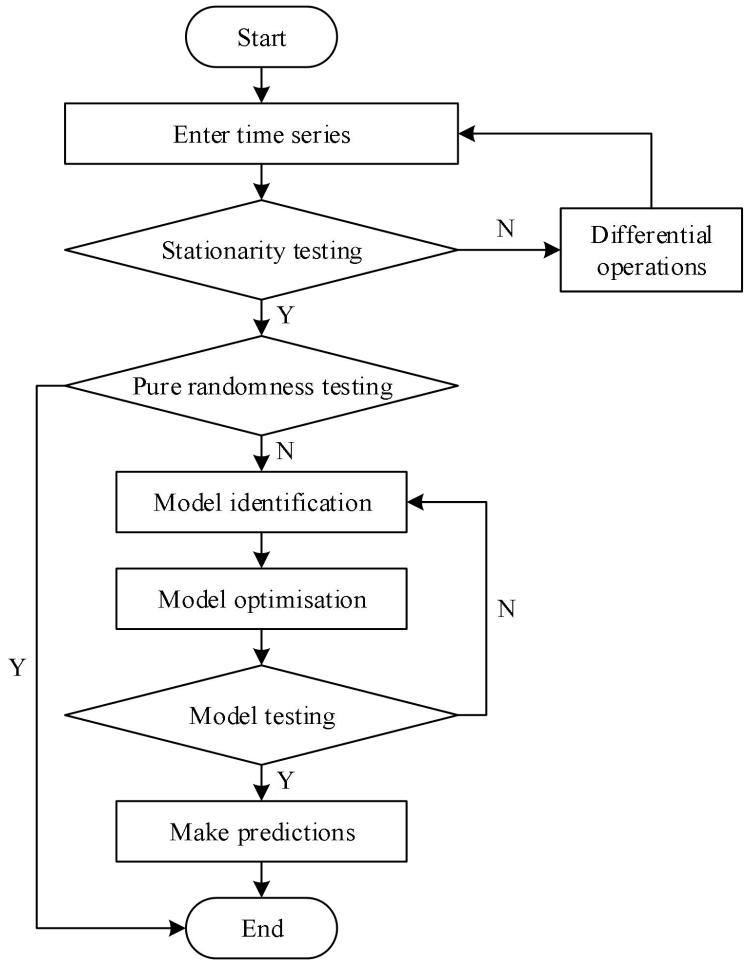

Figure 1. The ARIMA model builds the process.

2.2. LSTM neural network simulation of public emergency elements

Long Short-Term Memory (LSTM) neural network models [29] are a variant of recurrent neural networks (RNNs) [30]. Due to the vanishing gradient problem, RNNs can only have short-term memory, while LSTMs overcome this issue by introducing explicitly defined memory units and gate structures.

When using the LSTM neural network to simulate and estimate the response time elements of public emergencies, it is first necessary to confirm the model inputs, using historical public emergency response time data as the input variables. Additionally, to enhance the simulation accuracy of the LSTM model for public emergency response time data, the input data must be preprocessed before being fed into the model. The preprocessed public emergency response time data is then input into the LSTM neural network for training. The trained model outputs simulated values for public emergency response time data. By comparing the simulated public emergency response time data with actual public emergency response time data, the model's simulation effectiveness for public emergency response time elements can be evaluated. The model structure is shown in Figure 2, illustrating the process of using an LSTM neural network to simulate and estimate public emergency response time elements.

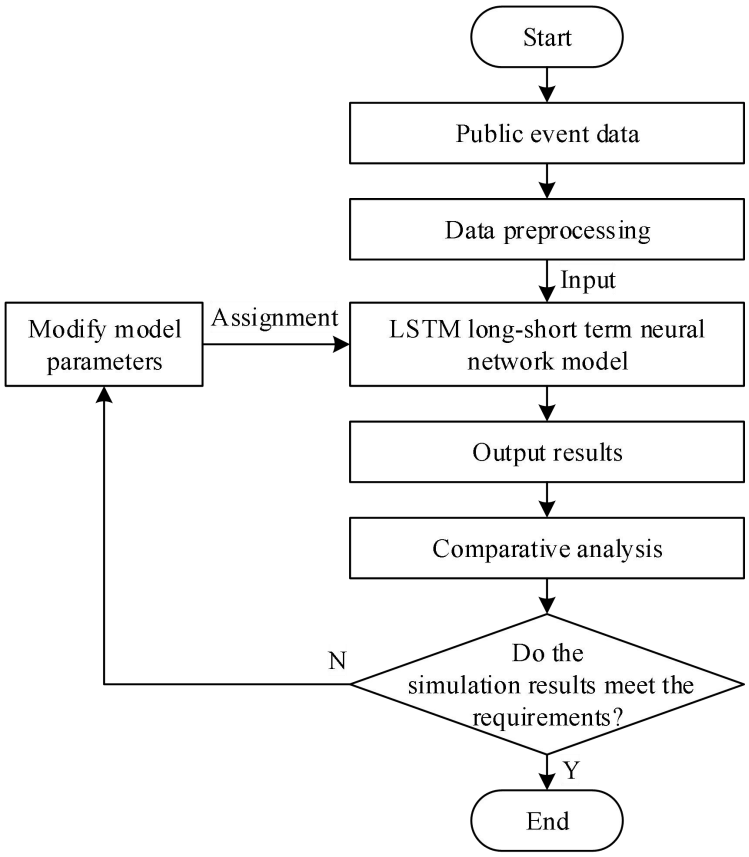

Figure 2. LSTM long term memory neural network data simulation process.

The following are the principles related to long-term and short-term memory neural networks:

The LSTM neural network has three inputs to the hidden layer, namely the unit state c_{t-1} at the previous moment, the output value s_t at the previous moment, and the current input value x_t.

The management and control of the cell state c is the key to the LSTM neural network's ability to store information in long-term memory. LSTM achieves this control by introducing three gate structures: the forget gate, the input gate, and the output gate.

(1) The forget gate is used to control the information that needs to be stored in the current cell state c_t from the cell state c_{t-1} at the previous moment. The expression is as follows:

$$f_t = \sigma\left(W_f \cdot \left[s_{t-1}, x_t\right] + b_f\right) \tag{7}$$

In the equation, W_f is the weight matrix of the forget gate, σ is the sigmoid activation function of the forget gate, b_f is the bias of the forget gate, x_t is the input at the current time step, and s_{t-1} is the unit state at the previous time step. The final value f_t is a value in the range $\left[0,1\right]$. If $f_t = 1$, it indicates that the previous time step's cell state is fully remembered; conversely, if $f_t = 0$, it indicates that the previous time step's cell state is fully forgotten. The value of f_t is generally in the range $\left(0,1\right)$, and only the information that needs to be retained from the previous time step's cell state is remembered.

(2) The input gate controls how much information from the current time step's input x_t is retained in the current cell state c_t, as expressed by the following equation:

$$i_t = \sigma\left(W_i \cdot \left[s_{t-1}, x_t\right] + b_i\right) \tag{8}$$

In the equation, W_i is the weight matrix of the forget gate, σ is the sigmoid activation function of

the forget gate, b_i is the bias of the forget gate, x_t is the input at the current time step, and s_{t-1} is the state of the unit at the previous time step. The final value i_t is a value in the range $[0,1]$. If $i_t = 1$, it indicates that all of the current input is remembered; conversely, if $i_t = 0$, it indicates that all of the current input is forgotten. The value of i_t is generally in the range $(0,1)$, and only the information that needs to be retained from the current input is remembered.

(3) Obtaining the candidate value vector $\tilde{c}_t$ for the current cell state is a prerequisite for obtaining the current cell state c_t. The expression for $\tilde{c}_t$ is as follows:

$$\tilde{c}_t = \tanh\left(W_C \cdot [s_{t-1}, x_t] + b_C\right) \tag{9}$$

In the equation, W_c is the weight matrix of the forget gate, $\tanh$ is the activation function of the forget gate, b_c is the bias of the forget gate, x_t is the input at the current time, and s_{t-1} is the unit state at the previous time. Finally, $\tilde{c}_t$ is obtained as a value in the range $[0,1]$.

(4) The expression for the current cell state c_t is shown in the following equation:

$$c_t = f_t * c_{t-1} + i_t * \tilde{c}_t \tag{10}$$

In the formula, c_{t-1} is the cell state at the previous moment, and $\tilde{c}_t$, i_t, f_t are the values at the current moment, all of which can be obtained through the above formula, so that the current memory and long-term memory can be integrated to obtain the current cell state c_t.

(5) The output gate controls the amount of information from the current cell state c_t stored in the current output s_t, as expressed by the following equation:

$$o_t = \sigma\left(W_o \cdot [s_{t-1}, x_t] + b_o\right) \tag{11}$$

$$s_t = o_t * \tanh\left(c_t\right) \tag{12}$$

W_o is the weight matrix of the forget gate, σ is the sigmoid activation function of the forget gate, b_o is the bias of the forget gate, x_t is the input at the current time step, s_{t-1} is the unit state at the previous time step, and the final output o_t is a value in the range $[0,1]$. Finally, the current cell is combined with the output gate to obtain o_t, resulting in the current output s_t.

2.3. Building an ARIMA-LSTM combination measurement model

Based on the confirmation that both the ARIMA time series model and the LSTM neural network model can effectively simulate public emergency response time data, to further enhance the simulation accuracy of public emergency response time data and reduce the prediction error in this study, we combined the ARIMA and LSTM models using an optimal weighted combination prediction method based on the simulation results of the two single models and the actual values of the public emergency response time data. This approach aims to obtain a more reliable and objective combined model, thereby effectively improving the simulation accuracy of public emergency response time elements.

The purpose of constructing the ARIMA-LSTM combined model [31] is primarily to comprehensively utilize the information provided by each single model to maximize the simulation prediction accuracy of public emergency response time elements. Theoretically, this combined model can provide a more comprehensive and systematic consideration of the problem compared to single models.

The method for determining the weighting coefficients of each individual model in the ARIMA-LSTM combined prediction model constructed in this paper is based on the minimum sum of squared errors criterion of the simulation prediction results of public emergency response time data from the combined model. The weighting coefficients of each individual model are calculated using a linear equation. By combining the ARIMA model and the LSTM neural network model, the combined measurement model can better simulate and predict changes in the response time elements of public emergencies. By comprehensively utilizing the information provided by multiple single models, the

accuracy of simulation and prediction is improved.

The specific methods and related calculation formulas for constructing the ARIMA-LSTM combined model are as follows:

Let A and L be the simulated prediction values of the ARIMA model and LSTM neural network model for the emergency response time elements of public emergencies, respectively, and let Y be the optimal combination prediction value. Their simulated prediction errors are E_a , E_1 , and E_y , respectively. According to the principle that the sum of squared prediction errors is minimized, i.e., minimizing $E = \sum E_y^{\ 2}$ is optimal, where K_a and K_1 are the corresponding weight coefficients $\left(K_a + K_1 = 1\right)$, the calculation formulas for E_y and Y are as follows:

$$E_y = K_a * E_a + K_1 * E_1 \tag{13}$$

$$Y = K_a A + K_1 L \tag{14}$$

The calculation equations for K_1 and K_a are:

$$K_l = 1 - K_a \tag{15}$$

$$K_a = -\frac{\sum\left(E_a - E_1\right)E_1}{\sum\left(E_a - E_1\right)^2} \tag{16}$$

$$RMSE = \left(\frac{1}{N}\sum_{i=1}^{N}\left(y_i - \hat{y}_i\right)^2\right)^{\frac{1}{2}} \tag{17}$$

By determining the weight ratios of the two single public emergency response time element measurement models—ARIMA time series and LSTM neural network—in the optimal combination model, the weighted ARIMA-LSTM combination measurement model is used to simulate and predict the time series of public emergency response time elements.

3. Performance testing of public emergency response event models

3.1. Data Sources

To validate the effectiveness of the proposed combination model, this section collects response time monitoring data from the State Grid Network University platform. The dataset covers the time period from June 1, 2020, to June 10, 2020, with a collection frequency of 4.8 minutes, resulting in 300 data points per day and a total of 3,000 data points over 10 days. Due to random factors (including network outages or server failures), the original data may contain outliers, which could mislead time series predictions. To reduce the impact of these outliers on the prediction process, this paper employs the classic box plot method to identify outliers, removing sequence values exceeding 1.5 times the sum of the interquartile range and the third quartile as outliers. For data missing at individual time points after outliers are removed, the average of the two adjacent time points' sequence values is used as the fill value. Observing the dataset reveals that data volatility is significant between 6 PM and 12 AM each day. Therefore, the 75 data points from 6 PM to 12 AM on the last day are used as the test set, while the remaining 2,925 data points form the training set.

3.2. Evaluation Indicators

This paper uses three representative evaluation error standards to assess the accuracy of predictions: root mean square error (RMSE), mean absolute percentage error (MAPE), and mean absolute error (MAE). Their mathematical expressions are as follows:

$$RMSE = \sqrt{\frac{1}{n}\times\sum_{i=1}^{n}\left(F_i - R_i\right)^2} \tag{18}$$

$$MAPE = \sum_{i=1}^{n}\left|\frac{F_i - R_i}{R_i}\right| \times \frac{100}{n} \tag{19}$$

$$MAE = \sum_{i=1}^{n} \frac{|F_i - R_i|}{n} \tag{20}$$

In this context, F_i denotes the i th predicted value, R_i is the i th true value, and n is the sequence length (number of sample points). Smaller values of RMSE, MAPE, and MAE indicate lower prediction errors, higher accuracy, and better model fitting capability.

3.3. Comparison of predicted response times to public emergencies

3.3.1. Establishment of ARIMA Model for Response Time Prediction

Figure 3 shows the time series plot of public emergency monitoring data. Figure 3(a) shows the raw data plot after preprocessing, from which it can be seen that the data has a certain periodicity and is a non-stationary sequence. Figure 3(b) shows the sequence plot after first-order differencing, from which it can be seen that the sequence data has been basically stabilized. ADF testing shows that the data has indeed reached the stability condition, so the model parameter d=1 is set.

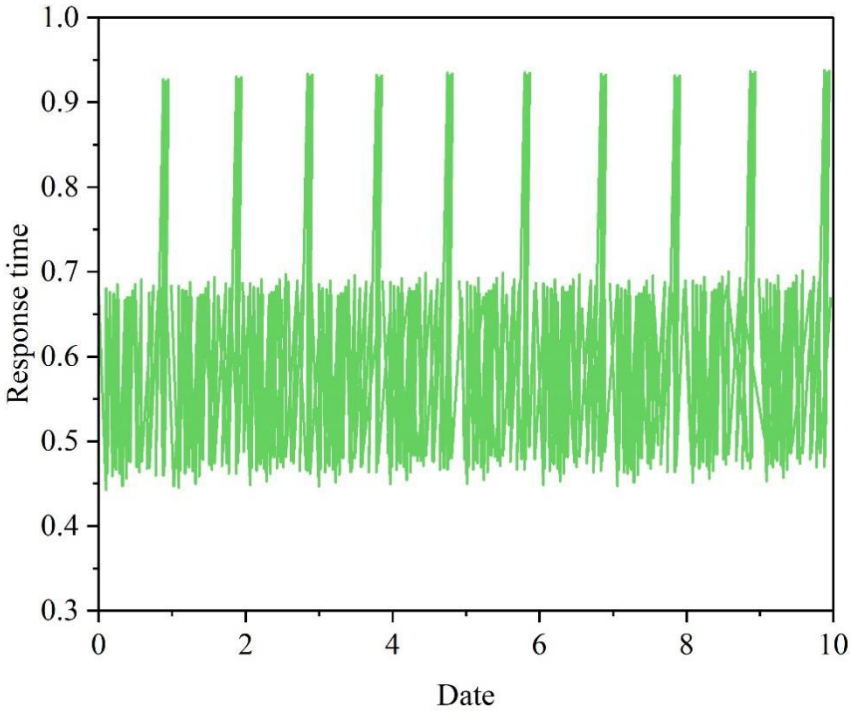

(a) Pre-processed data

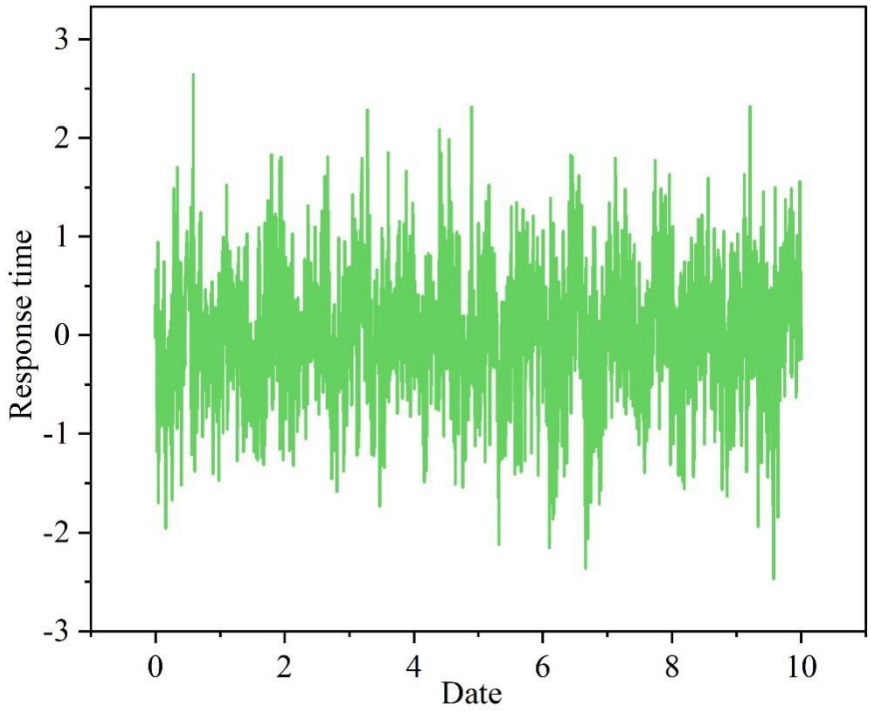

(b) The sequence of the first order difference treatment

Figure 3. Time sequence of public emergency monitoring data.

Then, based on the ACF plot and PACF plot, an initial judgment is made on the model parameters p and q. Figure 4 shows the autocorrelation analysis and partial autocorrelation analysis of the sequence data, with Figure 4(a) and Figure 4(b) displaying the ACF plot and PACF plot of the sequence data, respectively. From Figures 4(a) and 4(b), it can be observed that the ACF plot is truncated after lag 1, while the PACF plot is truncated after lag 3. Therefore, the maximum value for the ARIMA model parameter q is set to 1, and the maximum value for parameter p is set to 3. There are a total of 8 suitable model parameter combinations, namely (p, d, q) = (0, 1, 0), (0, 1, 1), (0, 1, 2), (0, 1, 3), (1, 1, 0), (1, 1, 1), (1, 1, 2), and (1, 1, 3). The BIC values for each model combination are then calculated. The results show that the BIC value for the parameter combination (1, 1, 2) is the smallest, at 172.05. Therefore, the (1, 1, 2) parameter combination is selected to construct the ARIMA model, and predictions are made for the test set of response time data.

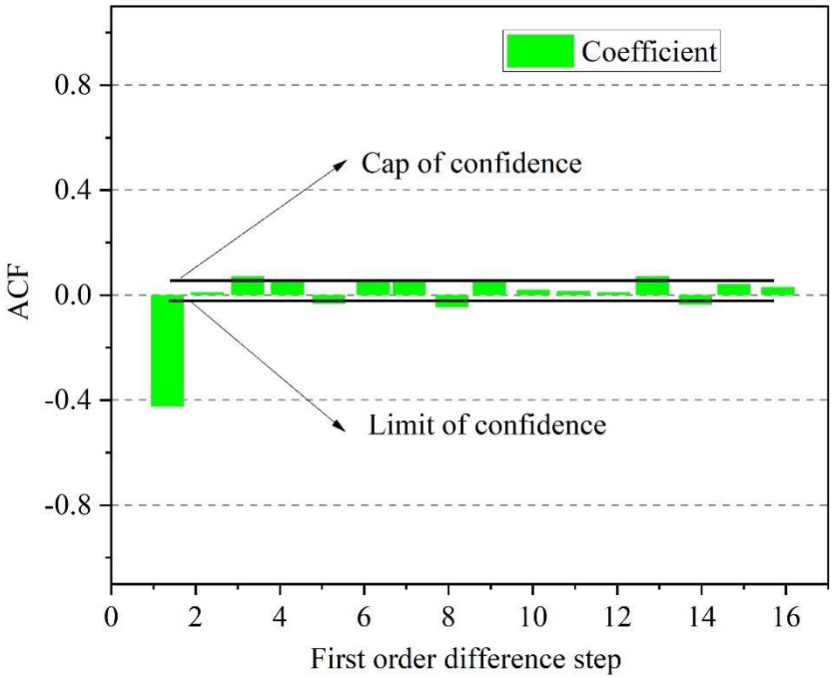

(a) ACF

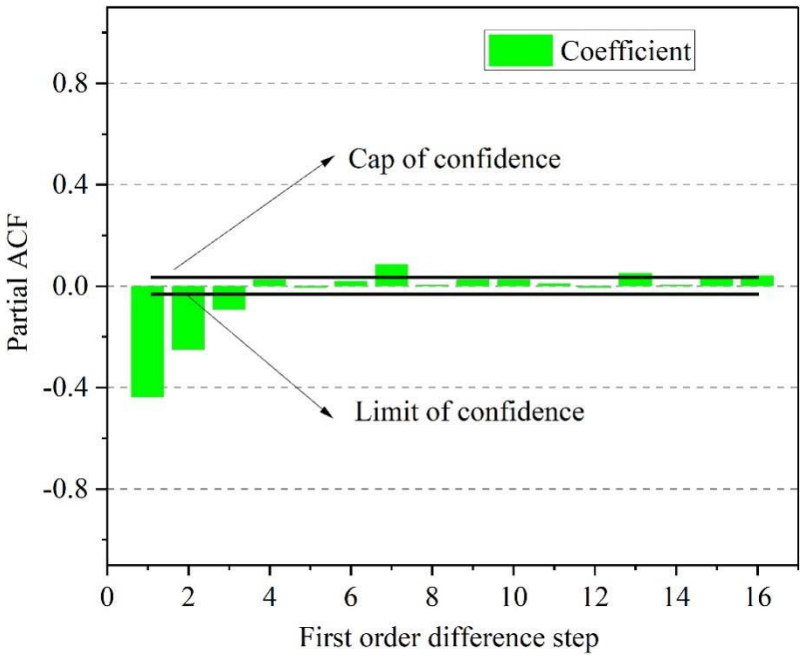

(b) PACF

Figure 4. Self-correlation analysis and partial self-correlation analysis.

3.3.2. LSTM parameter settings for predicting ARIMA residuals

The experimental platform uses the Keras framework. Based on experience and multiple residual experiments, the parameters of the LSTM model are set as follows. The number of input neurons is 3, the hidden layer is set to a single hidden layer with 400 neurons, the number of iterations (epochs) is 3000, and the batch size is 60. To further prevent overfitting, the dropout technique is used in model training. The loss rate for this experimental model is set to 0.08, meaning that 8% of the nodes are discarded during each round of weight updates. The loss function is the mean squared error (MSE), the activation function is ReLU, and the optimizer parameter is RMSprop.

3.3.3. Comparison of prediction results from different models

To visually compare the performance of different algorithms, Figure 5 shows the prediction results of various models. The horizontal axis "time" represents time points from 6 PM to 12 PM on June 10, 2018 (a total of 6 hours, 75 time points, with each time point spaced 4.8 minutes apart), while the vertical axis shows the corresponding response time values for each time point. As shown in Figure 5, the ARIMA algorithm exhibits significant lag in its prediction results, and its fitting performance deteriorates sharply as time progresses, particularly after time point 54. The BP model performs better than the ARIMA algorithm, but the LSTM model and the ARIMA-LSTMA combination model demonstrate superior fitting performance. This also highlights the outstanding performance of the LSTM model in single prediction models. Compared to the single LSTM model, the ARIMA-LSTM combination model has better fitting performance and higher prediction accuracy.

Table 1 compares the RMSE, MAPE, and MAE values of the prediction results for each model. The prediction accuracy of the BP model is similar to that of the ARIMA model. The LSTM model has lower values than the BP model and ARIMA model across all metrics, with significant differences, indicating that the LSTM model performs better than the previous two models in time series prediction. The combined ARIMA-LSTM model has significantly lower RMSE and MAE values than the LSTM model, and its MAPE value is also 0.012 lower than that of the LSTM model, indicating that the combined ARIMA-LSTM model has higher prediction accuracy than the LSTM model. Overall, the proposed combined ARIMA-LSTM model has the highest prediction accuracy and optimal performance.

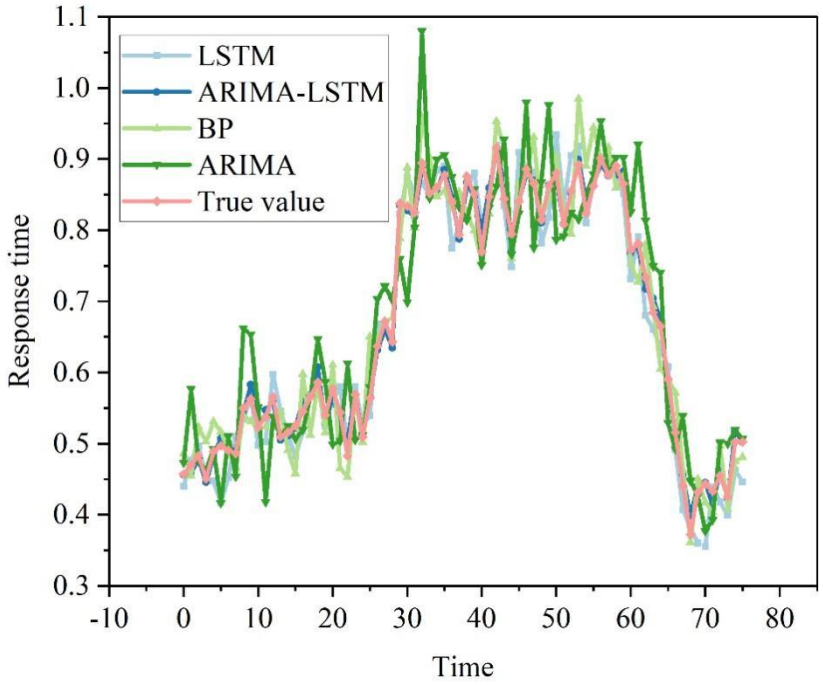

Figure 5. Prediction of different models.

Table 1. Compare the results of each model.

Model	RMSE	MAPE	MAE
BP	1.225	1.336	0.641
ARIMA	1.091	1.423	0.485
LSTM	0.218	0.082	0.152
ARIMA-LSTM	0.094	0.070	0.045

4. Application examples of public emergency response event models

4.1. Data Sources

The number of warning signals and the results of their handling from 2010 to 2024 in City P were

collected through the public emergency response event model. Data on public health emergencies were obtained from the public health emergency system.

4.2. Predicted response times for public emergencies

4.2.1. Overview of Forecasts

From 2010 to 2024, the five counties and districts of P City received a total of 12,200 warning signals, with 12,200 initial assessments. Among these, the single-case method accounted for 15% (1,830 cases), the time-based model method accounted for 60% (7,320 cases), and the spatio-temporal model method accounted for 25% (3,035 cases). The response rate was 100.0%, with an 88% timely response rate (10,736 alerts). The positive rate for suspected events was 2% (244), and the positive rate for outbreak events was 0.5% (61).

4.2.2. Distribution of diseases

The response to early warning signals using the single-case method is shown in Table 2. From 2010 to 2024, the early warning signals generated by the prediction system primarily focused on respiratory and intestinal infectious diseases, involving a total of 28 disease types. The single-case method covered 15 disease types (1,830 cases), with the top three being pneumonia, measles, and novel coronavirus infection, accounting for 78.31% of all warning signals. The positive rate for suspected events was 7.65%, with the top three diseases being human infection with H7N9 avian influenza, human infection with highly pathogenic avian influenza, and novel coronavirus infection. The positive rate for outbreak events was 1.91%, with the top three diseases being dengue fever, novel coronavirus infection, and pulmonary tuberculosis.

Table 2. A single case method warning signal response.

Warning disease	Warning number	Suspected incident	Outbreak
Tuberculosis	735	14	4
Measles	442	12	1
New coronary virus infection	356	108	28
Foot-and-mouth disease	150	0	0
Malaria	108	0	0
Dengue fever	10	2	2
Unknown cause pneumonia	7	1	0
Filariasis	6	0	0
Infectious SARS	4	0	0
Cholera	3	0	0
Schistosomiasis	2	0	0
People are infected with highly pathogenic avian influenza	2	1	0
H7N9 bird flu	2	2	0
Anthrax lung	2	0	0
Wolf pox	1	0	0
Total	1830	140	35

The response to early warning signals using the time model method is shown in Table 3. The time model method covers 17 disease types, with the top three being other infectious diarrhea diseases, dysentery, and hand, foot, and mouth disease, accounting for 71.48% of the total early warnings. The positive rate for suspected events was 0.66%, with the top three diseases being measles, rubella, and influenza. The positive rate for outbreak events was 0.19%, with the top three diseases being rubella, influenza, and hand, foot, and mouth disease.

Table 3. Time model method warning signal response.

Warning disease	Warning number	Suspected incident	Outbreak
Other infectious diarrhoeal diseases	2150	1	0
Dysentery	2082	0	0
Foot-and-mouth disease	1000	4	2
Mumps	900	15	1
Influenza	602	17	7

Scarlet fever	193	0	0
Hepatitis a	165	0	0
Hepatitis c	70	0	0
Amyl	35	0	0
Rubella	31	4	4
Typhus	17	0	0
New coronary virus infection	11	0	0
Acute hemorrhage conjunctivitis	10	0	0
Measles	8	7	0
Malaria	5	0	0
Typhoid typhus	3	0	0
Ideencephalon	2	0	0
Total	7320	48	14

The response to early warning signals using the spatiotemporal modeling method is shown in Table 4. The spatiotemporal modeling method covers 13 disease types, with the top three being other infectious diarrhea, mumps, and dysentery, accounting for 78.15% of the total early warnings. The positive rate for suspected events was 2.08%, with the top three diseases being rubella, influenza, and mumps. The positive rate for outbreak events was 0.86%, with the diseases being rubella and influenza. The differences in the positive rates for suspected events ($\chi^2 = 347.18$, $P < 0.01$) and outbreak events ($\chi^2 = 84.61$, $P < 0.01$) among the three warning methods were statistically significant.

Table 4. Temporal model method.

Warning disease	Warning number	Suspected incident	Outbreak
Other infectious diarrhoeal diseases	1072	0	0
Mumps	690	21	0
Dysentery	610	0	0
Influenza	392	35	20
Hepatitis a	100	0	0
Hepatitis c	70	0	0
Scarlet fever	42	1	0
Rubella	23	6	6
Typhus	18	0	0
Measles	8	0	0
Amyl	4	0	0
Ideencephalon	3	0	0
Acute hemorrhage conjunctivitis	3	0	0
Total	3035	63	26

4.2.3. Time Distribution

The temporal distribution of infectious disease early warning signals is shown in Figure 6. Among the 12,200 early warning signals, the highest number was recorded in 2010, and the lowest in 2012. With an annual average of 813.33 signals. Over the 15-year period, the response rate within 24 hours showed an upward trend (trend $\chi^2 = 2022.58$, $P < 0.01$), with a 100.0% response rate within 24 hours in both 2022 and 2024. There were extreme values in the response time for warning signals, with the longest median response time occurring in 2011 and the shortest in 2019. The response time was negatively correlated with the year ($r^s = -0.36$, $P < 0.05$). The highest positive rate for suspected events was in 2023 (13.8%), and the highest positive rate for outbreak events was in 2021 (2.6%). There were statistically significant differences in the positive rates of suspected events ($\chi^2 = 510.98$, $P < 0.05$) and outbreak events ($\chi^2 = 105.11$, $P < 0.05$) between different years.

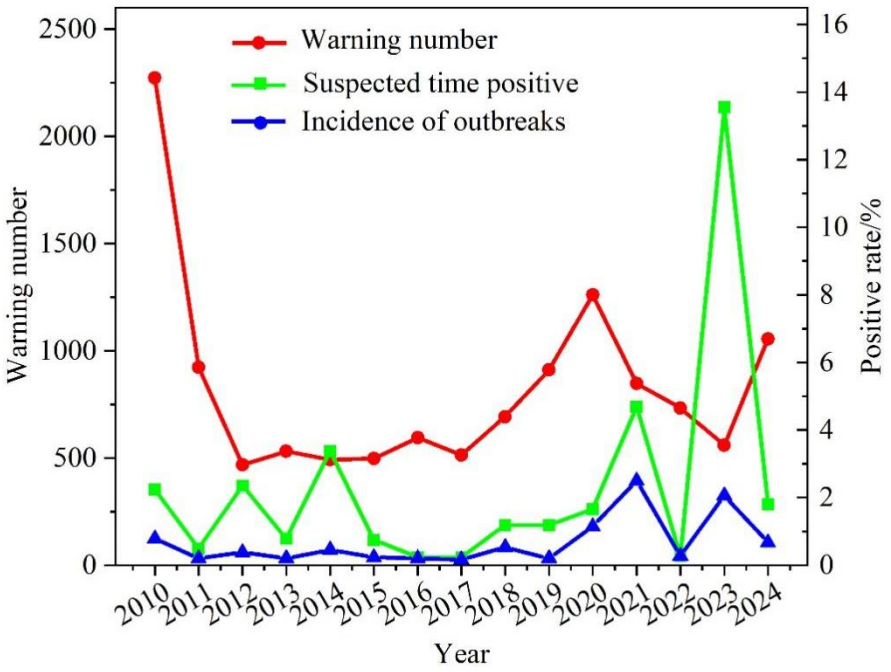

Figure 6. The distribution of automatic warning signals of infectious diseases.

4.2.4. Regional Distribution

The distribution of signal response rates across regions is shown in Table 5. The signal response rates for the infectious disease automatic prediction system were all 100.0% across the five counties and districts. Region A had the highest proportion of warning signals (29.51%), followed by Region B (24.18%) and Region C (18.69%), together accounting for 72.38% of the total warning signals. The top three regions with the highest positive rates for suspected events are Region E, Region B, and Region C. The top three regions with the highest positive rates for outbreak events were Region E, Region B, and Region D. The differences in positive rates for suspected events (χ^2 = 21.12, P < 0.05) and outbreak events (χ^2 = 30.45, P < 0.05) across different counties and districts were statistically significant.

Table 5. Signal response area distribution.

Area number	Warning number	Suspected incident	Outbreak
A	3600	60	11
B	2950	68	31
C	2280	48	0
D	1950	15	10
E	1420	50	16
Total	12200	241	68

4.2.5. Results of Early Warning Response Time Analysis

Table 6 presents the results of the early warning response time analysis. From 2010 to 2024, all early warning signals were responded to, with a response rate of 100.0%. The response rates for <2h, <24h, and ≥24h were 58.43%, 86.82%, and 13.18%, respectively.

The average early warning signal response time was 2.3 hours. During weekdays from 2010 to 2024, the response time for early warning signals was 1.4 hours, while on weekends and holidays, it was 2.8 hours. The difference in response times between weekdays and weekends/holidays was statistically significant after a rank-sum test (W = 12,022,315.0, P < 0.05).

The predictive model in this study can reduce the emergency response time for public emergencies.

The response time for 86.82% of events was less than 24 hours, significantly improving the timeliness of emergency responses, minimizing the loss of life and property caused by emergencies, and reducing their social impact, thereby providing technical support for social stability.

Table 6. Warning response.

Year	Warning total	Warning response number			Average response time (h)
		<2h	<24h	≥24h	
2010	2275	820	1540	735	4.1
2011	920	300	575	345	7.2
2012	452	170	350	102	3.6
2013	512	205	400	112	3.3
2014	485	175	365	120	3.8
2015	490	202	440	50	2.7
2016	588	389	577	11	1.1
2017	495	326	490	5	1.3
2018	680	505	675	5	0.9
2019	908	685	898	10	0.9
2020	1250	950	1245	5	1.0
2021	835	600	733	102	1.0
2022	720	505	720	0	1.0
2023	550	411	544	6	0.9
2024	1040	885	1040	0	0.9
Total	12200	7128	10592	1608	2.3

5. Conclusion

This paper proposes a public emergency response time prediction model based on a combination of ARIMA and LSTM models.

The model's predictive performance was studied using monitoring data from the State Grid Network University platform. The experimental results show that compared with the comparison models BP, ARIMA, and LSTM, the ARIMA-LSTM combination model proposed in this paper has better predictive performance, with a MAPE value that is 0.012 lower than that of the LSTM model, which has relatively good performance.

The emergency response warning signals for public emergencies in City P from 2010 to 2024 covered all five counties (districts) in the city. The positive rates for suspected events and outbreak events in the warning signals for counties A, B, C, D, and E were all low, not exceeding 5%. The average warning signal response time of the prediction model is 2.3 hours, with 86.82% of events responding within 24 hours, indicating that the model ensures most public emergencies are responded to within the 24-hour window. This provides critical information to relevant departments, maximizing efficiency in compressing public emergency response times, significantly enhancing the timeliness of emergency responses, and minimizing losses caused by public emergencies.

References

1. Xie, Y., Qiao, R., Shao, G., & Chen, H. (2017). Research on Chinese social media users' communication behaviors during public emergency events. Telematics and Informatics, 34(3), 740-754.
2. Savoia, E., Lin, L., & Viswanath, K. (2013). Communications in public health emergency preparedness: a systematic review of the literature. Biosecurity and bioterrorism: biodefense strategy, practice, and science, 11(3), 170-184.
3. Zhang, L., Zhao, W., Sun, B., Huang, Y., & Glänzel, W. (2020). How scientific research reacts to international

public health emergencies: a global analysis of response patterns. Scientometrics, 124(1), 747-773.
4. Seeger, M. W., Pechta, L. E., Price, S. M., Lubell, K. M., Rose, D. A., Sapru, S., ... & Smith, B. J. (2018). A conceptual model for evaluating emergency risk communication in public health. Health security, 16(3), 193-203.
5. World Health Organization. (2018). Communicating risk in public health emergencies: a WHO guideline for emergency risk communication (ERC) policy and practice. In Communicating risk in public health emergencies: a WHO guideline for emergency risk communication (ERC) policy and practice.
6. Cruz, M. P., Santos, E., Cervantes, M. V., & Juárez, M. L. (2021). COVID-19, a worldwide public health emergency. Revista Clínica Española (English Edition), 221(1), 55-61.
7. Morris, J. T., Mueller, J. L., & Jones, M. L. (2014). Use of social media during public emergencies by people with disabilities. Western journal of emergency medicine, 15(5), 567.
8. Wilder-Smith, A., & Osman, S. (2020). Public health emergencies of international concern: a historic overview. Journal of travel medicine, 27(8), taaa227.
9. Gostin, L. O., & Hodge, J. G. (2020). US emergency legal responses to novel coronavirus: balancing public health and civil liberties. Jama, 323(12), 1131-1132.
10. Ramsbottom, A., O'Brien, E., Ciotti, L., & Takacs, J. (2018). Enablers and barriers to community engagement in public health emergency preparedness: a literature review. Journal of community health, 43(2), 412-420.
11. Van Houdt, G., Mosquera, C., & Nápoles, G. (2020). A review on the long short-term memory model. Artificial Intelligence Review, 53(8), 5929-5955.
12. Jia, X., Gavves, E., Fernando, B., & Tuytelaars, T. (2015). Guiding the long-short term memory model for image caption generation. In Proceedings of the IEEE international conference on computer vision (pp. 2407-2415).
13. Shao, W., Zhang, Y., Guo, B., Qin, K., Chan, J., & Salim, F. D. (2019). Parking availability prediction with long short term memory model. In Green, Pervasive, and Cloud Computing: 13th International Conference, GPC 2018, Hangzhou, China, May 11-13, 2018, Revised Selected Papers 13 (pp. 124-137). Springer International Publishing.
14. Tian, C., Ma, J., Zhang, C., & Zhan, P. (2018). A deep neural network model for short-term load forecast based on long short-term memory network and convolutional neural network. Energies, 11(12), 3493.
15. Wang, J., Zhang, J., & Wang, X. (2017). Bilateral LSTM: A two-dimensional long short-term memory model with multiply memory units for short-term cycle time forecasting in re-entrant manufacturing systems. IEEE Transactions on Industrial Informatics, 14(2), 748-758.
16. Wang, B., Kong, W., Guan, H., & Xiong, N. N. (2019). Air quality forecasting based on gated recurrent long short term memory model in Internet of Things. IEEE Access, 7, 69524-69534.
17. Norris, D. (2017). Short-term memory and long-term memory are still different. Psychological bulletin, 143(9), 992.
18. Kumar, A., Sangwan, S. R., Arora, A., Nayyar, A., & Abdel-Basset, M. (2019). Sarcasm detection using soft attention-based bidirectional long short-term memory model with convolution network. IEEE access, 7, 23319-23328.
19. Hancock, P. A. (2023). Reacting and responding to rare, uncertain and unprecedented events. Ergonomics, 66(4), 454-478.
20. Gale, R. P., Armitage, J. O., & Hashmi, S. K. (2021). Emergency response to radiological and nuclear accidents and incidents. British journal of haematology, 192(6), 968-972.
21. Yang, C. T., Chen, Y. A., Chan, Y. W., Lee, C. L., Tsan, Y. T., Chan, W. C., & Liu, P. Y. (2020). Influenza-like illness prediction using a long short-term memory deep learning model with multiple open data sources. The Journal of Supercomputing, 76, 9303-9329.
22. Zhai, W., & Cheng, C. (2020). A long short-term memory approach to predicting air quality based on social media data. Atmospheric Environment, 237, 117411.
23. Fernandes, F., Stefenon, S. F., Seman, L. O., Nied, A., Ferreira, F. C. S., Subtil, M. C. M., ... & Leithardt, V. R. Q. (2022). Long short-term memory stacking model to predict the number of cases and deaths caused by COVID-19. Journal of Intelligent & Fuzzy Systems, 42(6), 6221-6234.
24. Vieira Roque, F., Fröhlich, A. A., & Grellert, M. (2025). An LSTM approach to predict emergency events using spatial features. Applied Intelligence, 55(5), 334.
25. Mu, G., Liao, Z., Li, J., Qin, N., & Yang, Z. (2023). IPSO-LSTM hybrid model for predicting online public opinion trends in emergencies. PLoS One, 18(10), e0292677.
26. Chen, J., & Sun, B. (2024). Enhancing Financial Risk Prediction Using TG-LSTM Model: An Innovative Approach with Applications to Public Health Emergencies. Journal of the Knowledge Economy, 1-21.
27. Fang, H., Peng, M. J., Du, X. T., Lin, B. S., Jiang, M. J., & Hu, J. Y. (2024). Integrating Long Short-Term Memory and Multilayer Perception for an intelligent public affairs distribution model. Acadlore Trans. Mach. Learn, 3(3), 148-161.
28. David Muñoz Rodríguez,Manuel J. González Ortega,María Jesús Aguilera Ureña,Andrés Ortega Ballesteros & Alberto Jesus Perea Moreno. (2025). Innovation ARIMA models application to predict pressure variations in water supply networks with open-loop control. Case study in Noja (Cantabria, Spain). Energy Nexus,18,100423-100423.
29. Yumei Zhang & Changlong Liu. (2025). Melody prediction of vocal performance using LSTM and attention mechanism and its application in folk music innovation. Journal of Computational Methods in Sciences and Engineering,25(4),3608-3622.

30. Shuo Hao,Hong Wei Li,Yi Qing Ni,Weijia Zhang & Lei Yuan. (2025). State estimation in structural dynamics through RNN transfer learning. Mechanical Systems and Signal Processing,233,112767-112767.
31. Xuejun Li & Dianzheng Zhuang. (2025). Long-Term Trend Analysis and Prediction of Freight Volume in Beijing Using ARIMA-LSTM Model. International Core Journal of Engineering,11(5),9-17.